FINAL TECHNICAL REPORT

Award Number: 07HQGR0158

SOURCE PROCESSES OF BENIOFF ZONE AND CRUSTAL EARTHQUAKES OF THE ANCHORAGE-PRINCE WILLIAM SOUND REGION

Diane I. Doser
The University of Texas at El Paso, Department of Geological Sciences, 500 W. University Ave., El Paso, TX 79968
(915)-747-5851 (office), (915)-747-5073 (FAX), doser@geo.utep.edu

ABSTRACT:

This research focused on study of the source processes of M>5.0 historic and recent earthquakes of the Anchorage and Prince William Sound (PWS) region through empirical Greens function/relative source time function techniques that used smaller events as Greens functions for larger events. This has allowed us to estimate the stress drops, rupture directivity and source-time history of these earthquakes in order to determine how similar/different rupture histories are for earthquake sequences within the upper and lower plate source zones.

Introduction:

South-central Alaska (Figure 1) is one of the most complicated regions of interaction between the Pacific and North American plates. At the western edge of this region (Kodiak Island) subduction occurs between the Pacific and North American plates along the Aleutian megathrust, with subduction gradually transitioning to strike-slip motion along the Fairweather-Queen Charlotte fault system within southeastern Alaska (at ~135ºW).

In south-central Alaska the Pacific plate is being thrust beneath North America along the Aleutian megathrust at a rate of about 6.3 cm/yr (DeMets and Dixon, 1999). Plate motion is complicated by collision of the Yakutat block (Plafker, 1987), with North America (Figure 1). The buoyant Yakutat block resists subduction, resulting in the shallowing and abrupt change in strike of the plate interface beneath the Prince William Sound (PWS) region (Brocher et al., 1994). In 1964 a great earthquake (Mw=9.2) ruptured the plate boundary from the vicinity of PWS southwestward to the southern end of Kodiak Island (Figure 1). The greatest slip along the plate interface occurred along the PWS asperity (Figure 1), an asperity primarily controlled by the presence of the Yakutat Block. A second asperity in the Kodiak Island region also ruptured during the 1964 mainshock (Figure 1)

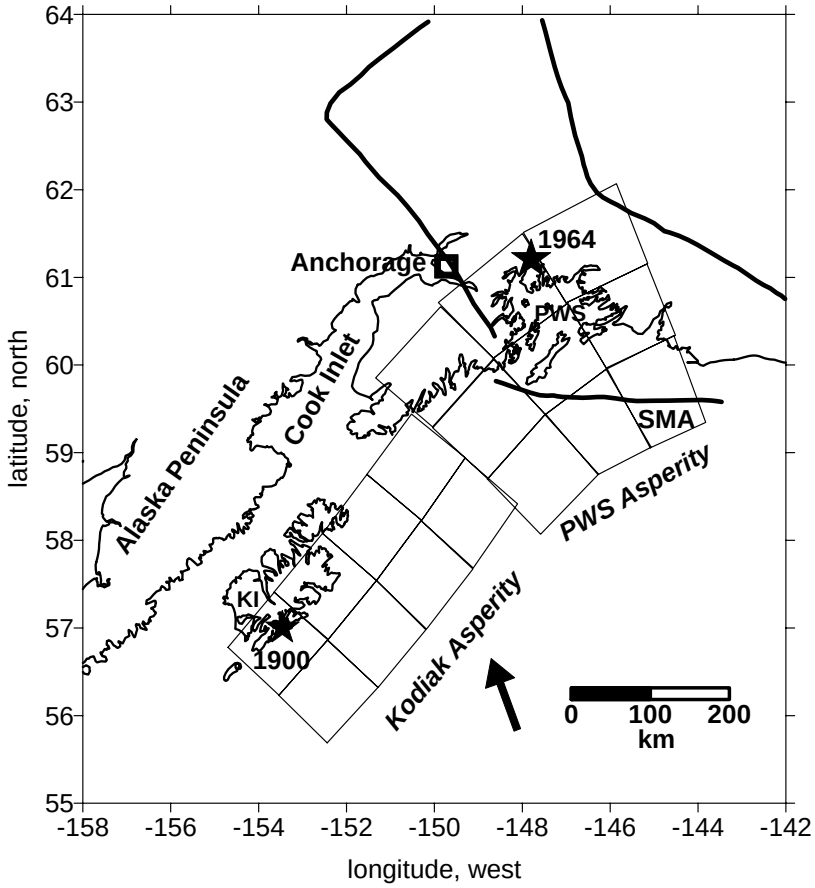

Figure 1 - Map of south-central Alaska showing the asperity model of Johnson et al. (1996) (rectangles). Bold lines indicate the position of the Yakutat block (Eberhart-Phillips et al., 2005). Star is epicenter of 1964 mainshock, square is the location of Anchorage. KI, Kodiak Island, PWS, Prince William Sound, SMA, slope magnetic anomaly defining the southern edge of Yakutat block.

The great Alaskan earthquake caused over $311 million (1964 dollars) in property loss, with most loss concentrated in the Anchorage area (Stover and Coffman, 1993). Although we do not expect to see a repeat of 1964 earthquake for 700 to 800 years (Wesson et al., 1999), other large (magnitude 6.5 to 7) earthquakes have caused MM intensities of up to VIII in the Anchorage and PWS regions. (In comparison, the 1964 mainshock produced average intensities of VIII at Anchorage, Seward and Valdez).

Because these earthquakes have smaller magnitudes, we would expect them to have shorter repeat times. Also the population and infrastructure of south-central Alaska have increased considerably since 1964. Thus the focus of this research was to better define the source properties (e.g. rupture directivity, stress drops) of these smaller magnitude crustal and Benioff zone earthquakes that are expected occur more frequently within the study area.

Empirical Greens function studies:

The empirical Greens function (EGF) technique is a method where a smaller event with a location and focal mechanism similar to a large event of interest (both recorded at the same station) is treated as a Greens function (representing the path effects between the source region and a station) and is deconvolved from the larger event. The result of the deconvolution, the

Relative Source Time Function (RSTF), provides information on the larger event's rupture history and rupture complexity (e.g. rupture directivity, variation of moment release, stress drop).

We analyzed the variations in RSTFs generated by moderate earthquakes (magnitudes 5 to 5.5) in south-central Alaska using data from strong motion and broadband seismograph stations. We hoped to determine if events in the more strongly coupled portion of the slab associated with the Prince William Sound asperity would have higher stress drops than slab events in less strongly coupled regions. We also wanted to compare stress drops and rupture directivity in slab events to those of crustal events.

Our area of study extended from 58° to 62°N and 144° to 154°W. Strong motion data for 13 events (Table 1) were obtained from the U.S. Geological Survey with the assistance Dr. Chris Stephens. Broadband data were obtained for an additional 27 events from the Incorporated Research Institutions in Seismology (IRIS) (Table 2). We selected events with depths < 100 km since events at these depths are the most likely to cause damage. Figure 2 shows the locations of the earthquakes recorded by the strong motion stations and Figure 3 shows the locations of earthquakes recorded by broadband stations.

Table 1. Moderate magnitude intraslab earthquakes recorded by strong motion instruments in south-central Alaska.

Date	Time	Latitude	Longitude	Depth (km)	M	Group
2002-02-06	17:18	61.17	-149.73	35	5.3	III
2002-02-06	17:19	61.18	-149.73	36	5.1	III
2002-05-27	02:53	61.35	-149.54	62	2.9	II
2003-12-15	14:55	61.35	-149.69	37	3.7	III
2004-08-23	07:19	61.81	-149.91	43	3.8	II
2004-08-25	02:22	61.59	-146.40	39	5.3	I
2004-10-06	18:31	61.48	-146.63	30	4.1	I
2005-01-29	16:37	60.13	-151.54	46	4.5	--
2005-02-16	18:35	61.33	-149.85	34	5.0	--
2005-04-06	17:51	61.45	-146.52	17	4.9	I
2005-04-06	22:42	61.45	-146.53	17	4.4	I
2005-04-17	21:33	60.76	-149.32	19	4.8	--
2005-11-19	01:18	61.51	-149.78	43	4.5	--

Table 2. Moderate magnitude intraslab earthquakes recorded by broadband stations.

Number	Date	Time	Latitude	Longitude	Depth	M_L
1	1999-04-18	15:05	60.39	-151.85	73	4.7
3	1999-05-05	10:30	59.31	-151.5	65.9	5.6
6	1999-07-03	15:26	61.44	-150.48	59.5	4.6
7	1999-07-22	05:35	61.31	-149.42	49.2	5.3
8	2000-02-27	02:22	60.3	-146.06	22.1	5.1
9	2000-03-01	23:05	60.29	-146.03	20.7	5.3
11	2000-03-16	08:48	61.45	-150.03	57.4	4.8
12	2000-06-15	03:03	59.34	-151.96	62.7	4.7

13	2001-03-23	13:38	59.54	-146.53	30.4	4.8
14	2002-02-06	17:18	61.2	-149.85	53.1	5.1
15	2002-02-06	17:19	61.24	-149.88	54.5	4.9
16	2002-02-25	21:19	60.54	-147.19	28.5	5.0
17	2002-08-06	19:53	61.51	-150.57	63.8	5.0
18	2003-02-12	00:50	59.47	-145.6	14.2	4.5
19	2004-02-10	20:33	59.47	-152.35	60.1	5.8
20	2004-03-05	09:25	60.58	-151.73	78	5.0
21	2004-06-21	21:29	61.76	-151.37	87.3	5.2
22	2004-08-25	02:22	61.67	-146.44	52.9	5.3
23	2004-12-21	17:21	60.55	-147.6	29.7	5.1
24	2005-01-13	17:36	60.51	-147.54	29.5	4.7
25	2005-02-16	18:35	61.37	-149.95	53.3	4.7
26	2005-04-06	17:51	61.54	-146.47	38	4.9
27	2005-04-17	21:33	60.83	-149.27	35.1	4.7
28	2005-05-19	01:12	60.02	-152.70	95.5	5.5
29	2006-02-05	16:15	59.39	-151.75	47.8	5.3
31	2007-10-03	14:06	58.28	-151.29	45.5	5.0
30	2007-11-28	23:57	61.91	-151.13	69.6	5.1

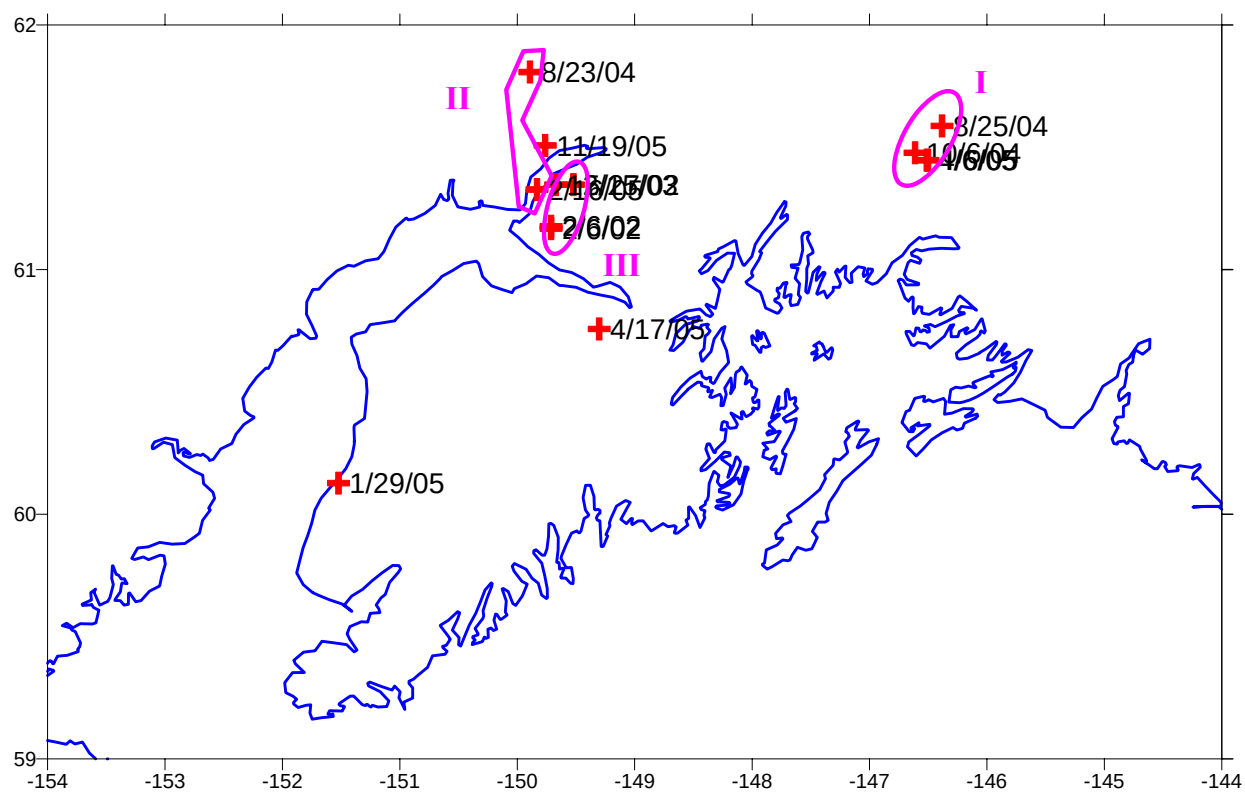

Figure 2 – Intraslab events recorded by strong motion instruments. Magenta lines surrounding events indicate groups used in EGF analysis (see Table 1).

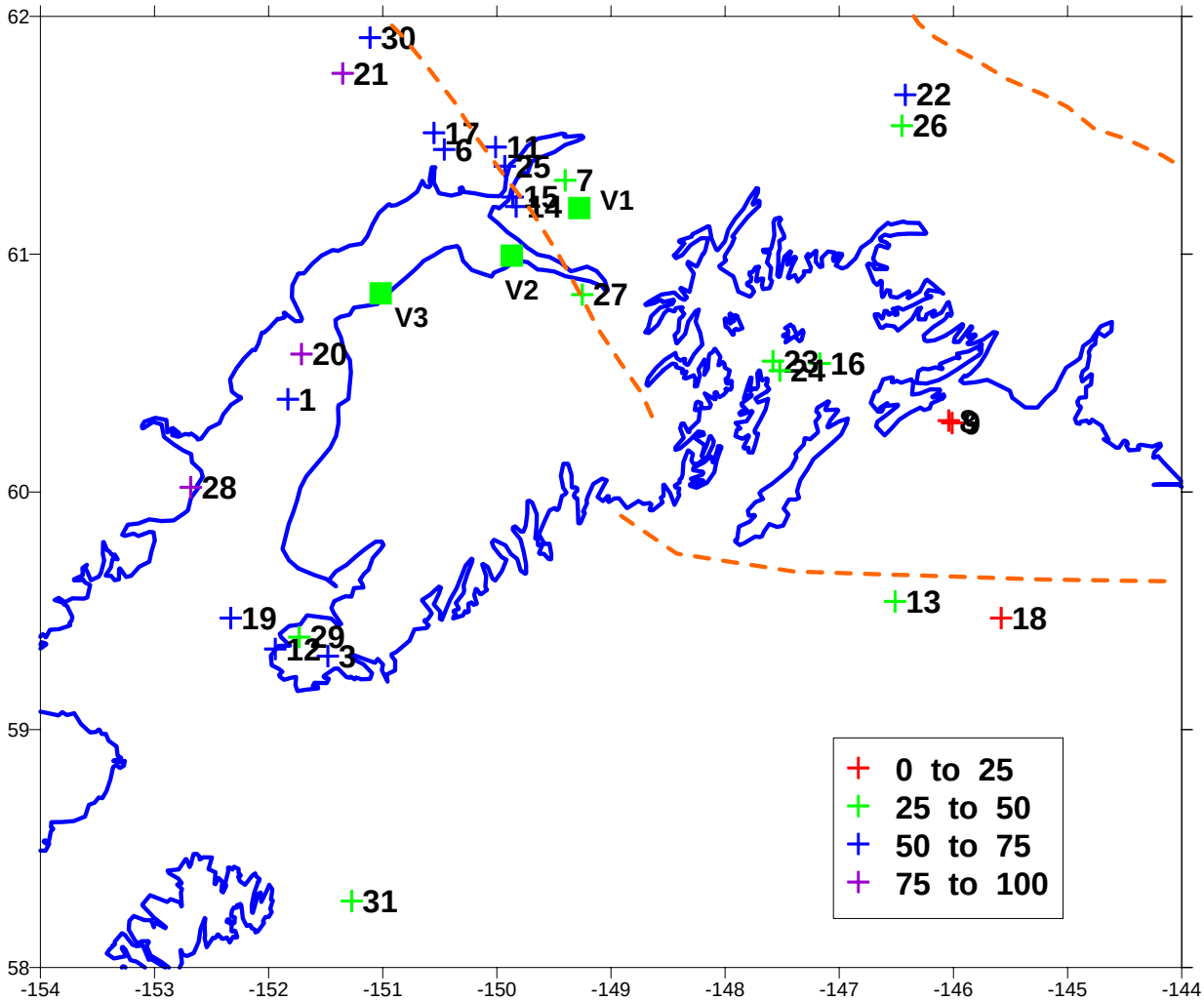

Figure 3. Map showing edges of Yakutat block (dashed orange lines) in south-central Alaska and events (crosses) recorded by broadband stations analyzed in this study. Symbol color indicates depth of events in km. Event numbers correspond to Table 2. Squares are events studied by Veilleux (2006).

Methodology

Calculation of RSTF's

The techniques we used for this study are primarily based on Muller (1985). We first select two seismograms recorded at the same station by the same instrument. One seismogram is from a larger magnitude event (mainshock) and the second event may represent an aftershock, foreshock or smaller event located near the mainshock. The latter seismogram is the EGF under the assumption that the smaller event has a focal mechanism similar to the mainshock. This assumption cancels the effects of path and instrument response for events recorded at the same station. Muller (1985) indicates that there must be a difference in magnitude of at least 1

between events. Next we take the spectral ratio of the mainshock to the EGF in the frequency domain. This operation isolates the source properties of the mainshock. We then transform the result to the time domain resulting in the RSTF.

In order to analyze the strong motion data, events in Table 1 were grouped into clusters as denoted by the regions in Figure 2. This grouping assumes that the events occurred close together in space and had similar focal mechanisms. Five events were located far enough apart or had dissimilar enough focal mechanisms that they could not be placed in a group (Table 1).

We illustrate an example of processing strong motion data in Figure 4. In this case we selected the M_L=5.3 earthquake occurring on August 25, 2004 as the mainshock and the M_L=4.1 earthquake on October 6, 2004 as the EGF (Table 1, Group I). Both events occurred at depths ~35 km with similar normal faulting mechanisms. The complete strong motion records are shown on the left and the windowed P-wave arrivals are shown on the right in Figure 4. The arrivals were selected using a cosine taper window. Figure 5 shows the spectral amplitudes of the two events (left) and the resulting spectral quotient (right). The spectral ratio was filtered in a narrow band of low frequencies (0.1 to 1 Hz) and was inversely transformed to the time domain. The time series obtained gives an RSTF (Figure 6) with duration of ~ 2 s.

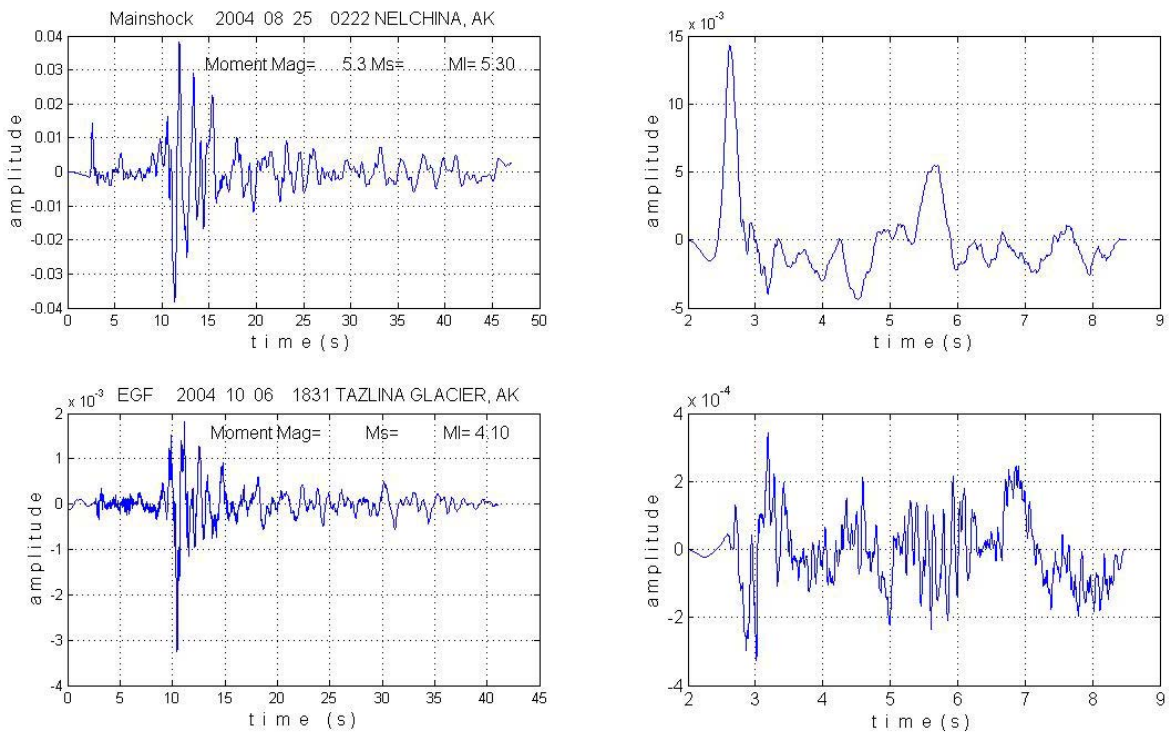

Figure 4. Whole event strong motion seismograms on the left and cosine taper windowed P-wave arrivals on the right.

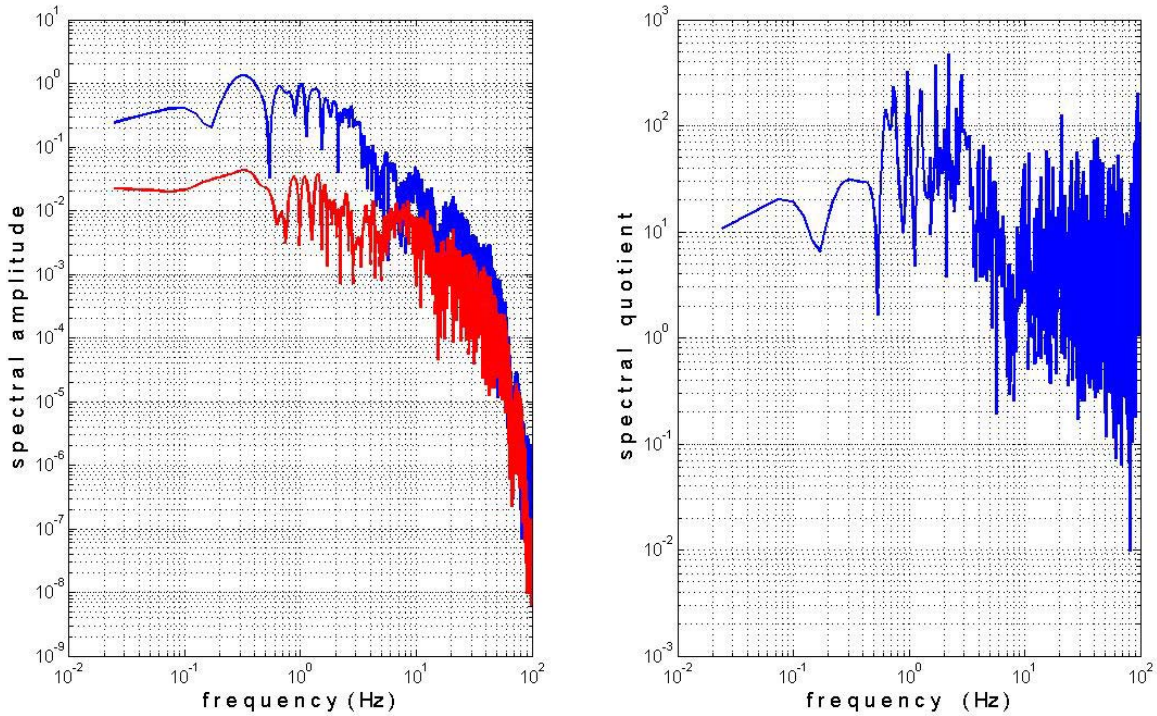

Figure 5. Spectral amplitudes of the mainshock (blue line) and EGF (red line) at left and the spectral ratio at right.

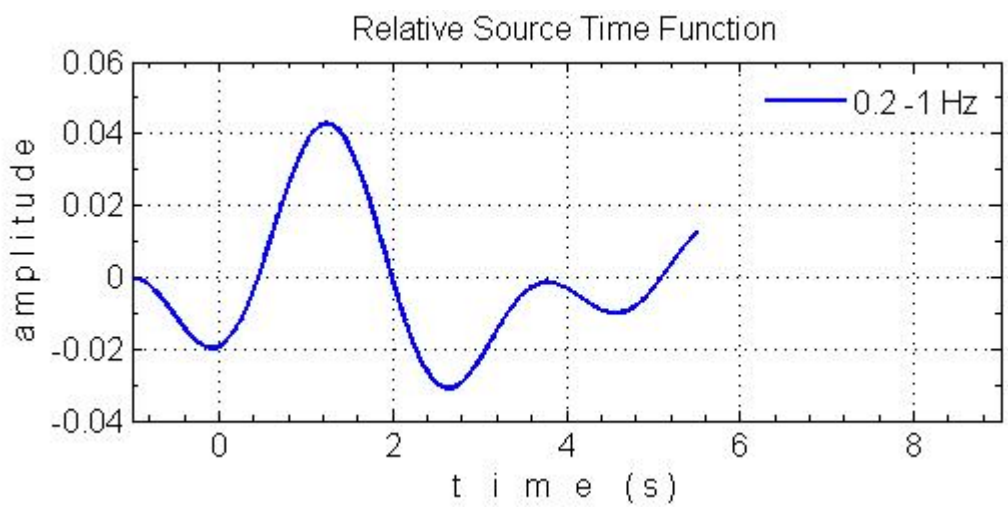

Figure 6. RSTF obtained for August 25, 2004 earthquake.

We used a similar procedure for the evaluation of RSTF's for broadband data. Figure 7 shows broadband seismograms for a pair of events on December 21, 2004 (mainshock) and January 13, 2005 (EGF). In this case we examined the effect of water levels on the spectral ratio. The left side of Figure 8 shows the observed spectral amplitudes for the mainshock and EGF and the right side shows the variation in spectral ratio with water level (c). Note that the figure indicates that the water level begins to affect the outcome when c > 0.01.

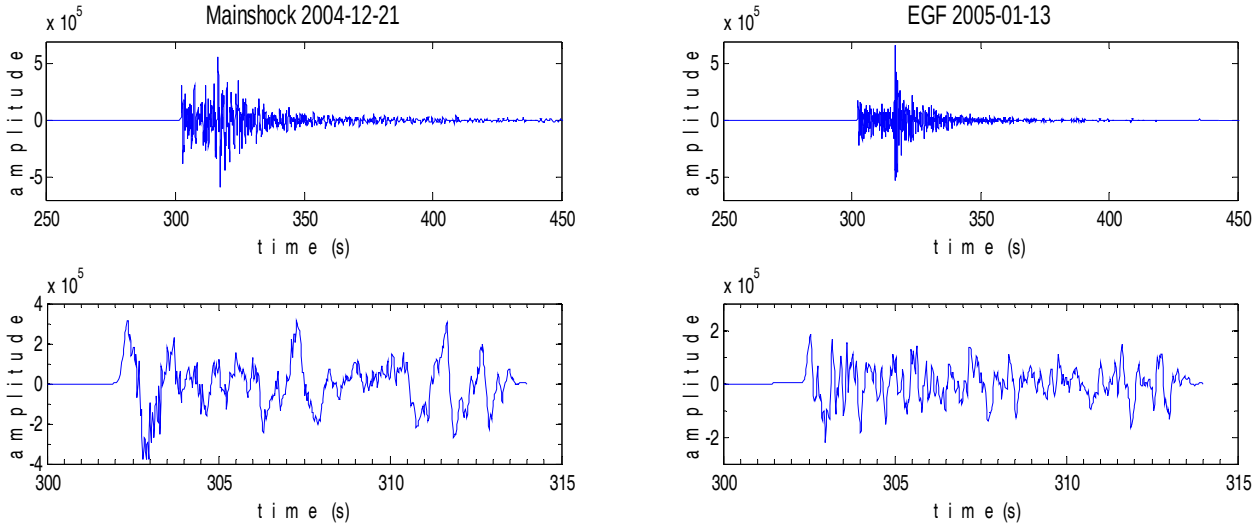

Figure 7. On top are broadband seismograms of the events at 2004-12-21 and 2005-01-13. At the bottom are the respective P-waves windowed with a taper cosine function.

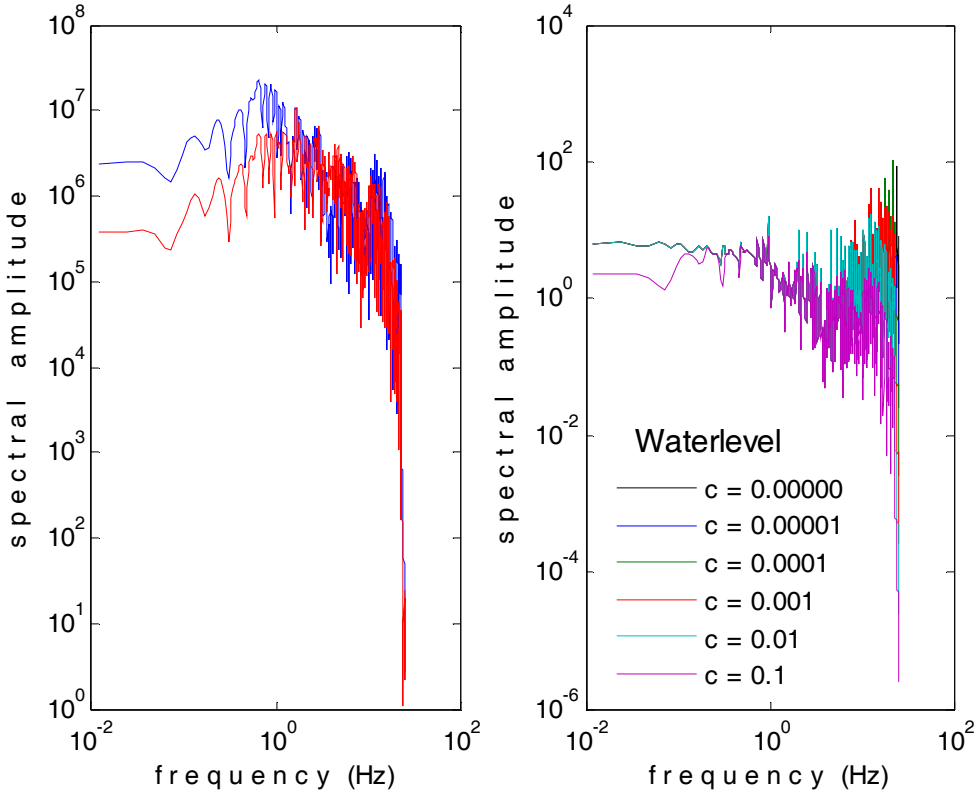

Figure 8. On the left, spectral amplitudes for the mainshock (blue) and the EGF (red). On the right the variation of spectral ratios with applied water level.

Determination of Stress Drops

The next step in our analysis was to estimate stress drops for the intraslab earthquakes. Stress drop ($\Delta\sigma$) is related to moment (M_0) and energy (E) through:

$$\Delta\sigma = \frac{2\mu E}{M_0} \qquad (1)$$

where μ is the shear modulus. The released energy is given by:

$$E = \frac{1}{5\pi\rho}\left(\frac{1}{3\alpha^5} + \frac{1}{2\beta^5}\right)\int_{-\infty}^{\infty}\left(\ddot{M}(t)\right)^2 dt \qquad (2)$$

with $\dot{M}(t)$ equal to the moment rate. In our case the moment rate function can be obtained from the RSTF ($R(t)$), but is must be scaled by the scalar seismic moment of the EGF. The substitution of (2) into (1) gives:

$$\Delta\sigma = \frac{2\mu}{5\pi\rho}\left(\frac{1}{3\alpha^5} + \frac{1}{2\beta^5}\right)\frac{\left(M_0^{EGF}\right)^2}{M^{Main}}\int_{-\infty}^{\infty}\left(\dot{R}(t)\right)^2 dt \qquad (3)$$

where ρ is density, α and β are P- and S-wave velocities at the point where the earthquake initiates and M_0^{EGF} and M_0^{Main} are the seismic moments of the EGF and mainshock, respectively. This equation has been used by Houston (1990) and Velasco et al. (1994a; 1994b), among others, to calculate dynamic stress drop and seismic energy. If we transform equation (3) to the frequency domain we obtain (Nava, 2002):

$$\Delta\sigma = \frac{16\pi}{5\rho}\left(\frac{1}{3\alpha^5} + \frac{1}{2\beta^5}\right)\frac{\left(M_0^{EGF}\right)^2}{M_0^{Main}}\int_{0}^{\infty} f^2\left|\hat{R}(f)\right|^2 df \qquad (4)$$

with $\hat{R}(f)$ representing the Fourier transform of $R(t)$. Although (3) and (4) should be equivalent, integration in the frequency domain is easier to accomplish and avoids the problem of anti-aliasing (Walter et al., 2006).

<u>Results:</u>

Strong motion data, intraslab events:

An example of the use of the RSTF analysis technique for strong motion data for two events of Group III (Table 1) is shown in Figure 9. In this case the February 6, 2002 was treated as the mainshock and the December 15, 2003 event was the EGF. Both events occurred nearly directly beneath Anchorage. The results (Figure 9) show the RSTF's at three stations located west of the mainshock and one station located northeast of the mainshock. Note that the RSTF's have a well defined impulsive shape for stations located to the west, while the RSTF shape for the station to the northeast is very different. These shapes suggest rupture towards the west or southwest.

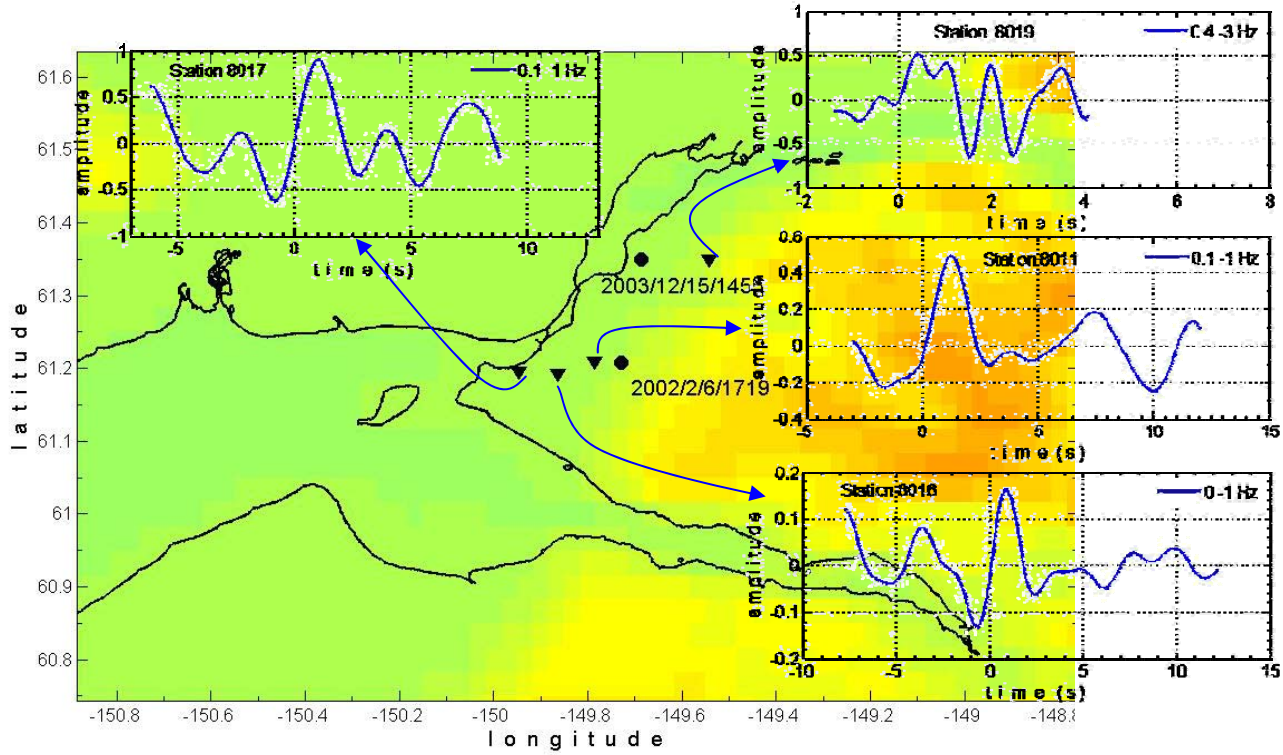

Figure 9. RSTFs obtained for the indicated strong motion stations for the event on February 6, 2002.

Although we were able to use strong motion data to obtain RSTF's, we usually had only 3 to 4 stations that could be used. Thus we did not feel we could as reliably determine stress drops with these data as compared to our broadband data where we usually had more than 7 RSTF's for each mainshock-EGF pair.

Broadband data, intraslab events:

Examples of RSTF estimates for three pairs of broadband events are shown in Figures 10 through 12. For most of our trials we were able to determine stable RSTF's. A stable RSTF could not be obtained for station BPAW for events 24 (EGF) and 23 (mainshock) (Figure 10), or for stations PPLA, PAX, and RC01 for events 26 (EGF) and 22 (mainshock) (Figure 11). Note that excellent RSTF's were obtained from the event pair 8 (EGF)/9 (mainshock) (Figure 12), however the poor azimuthal coverage does not allow for examination of source directivity.

Using equation (3) we estimated the dynamic stress drop for events 22, 23 and 24. For these events we used an average of all stacked RSTF's (see example in Figure 13 for event 23) to determine the stress drop. The RSTF's were stacked in such a way that all central maximums were in the same position. Stacking enhances the shape of the RSTF and diminishes the side lobes. Velasco (1994b) suggests that the stacked RSTF is the azimuthally averaged moment rate function and its squared derivative is proportional to energy release and hence stress drop. The derivative and squared derivative of the stacked RSTF for event 23 are shown in Figure 14.

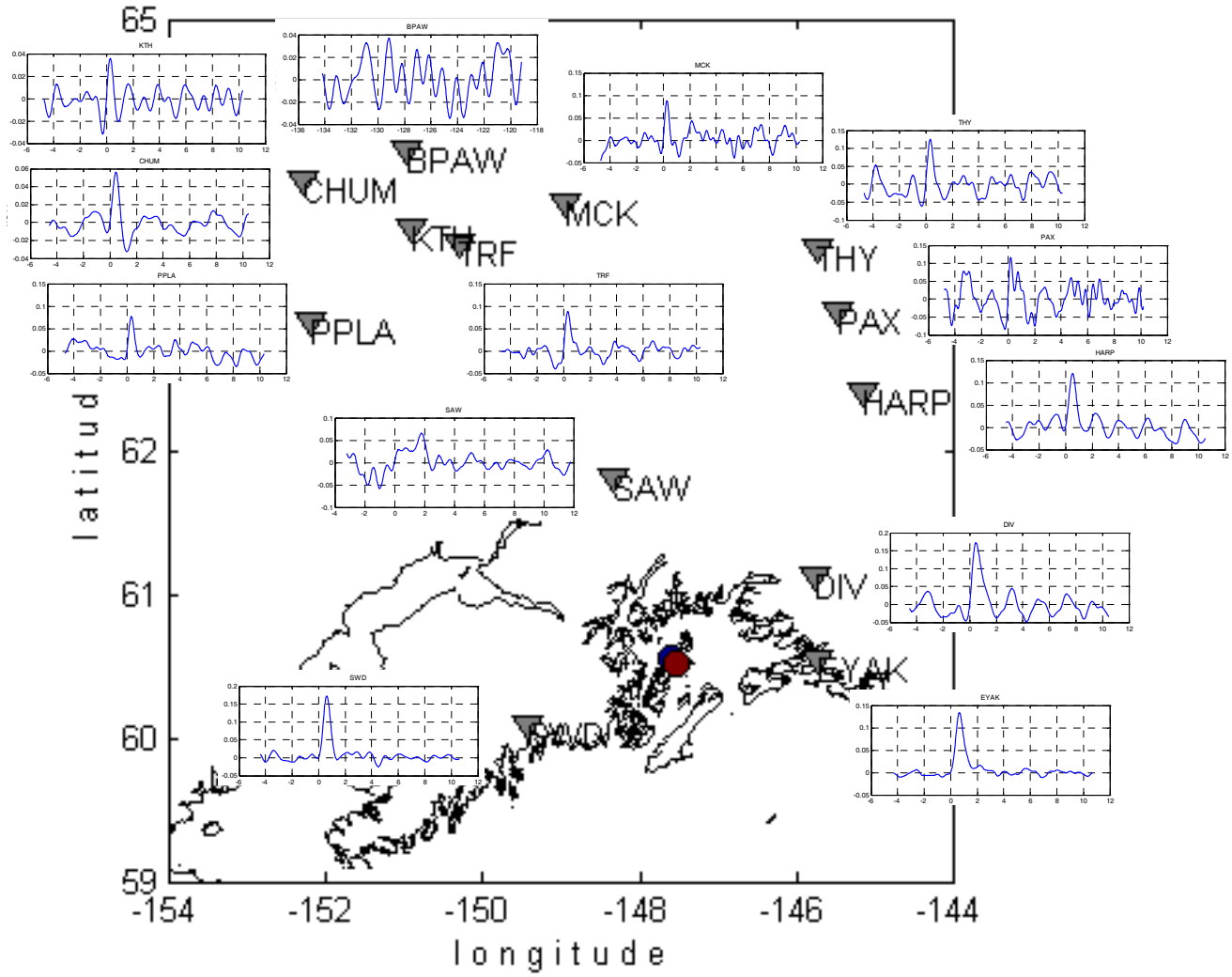

Figure 10. Variability of RSTFs depending on the azimuth from the event to the station (triangles). Event 23 is the mainshock and event 24 is the EGF (Table 2). Note the high instability at station BPAW.

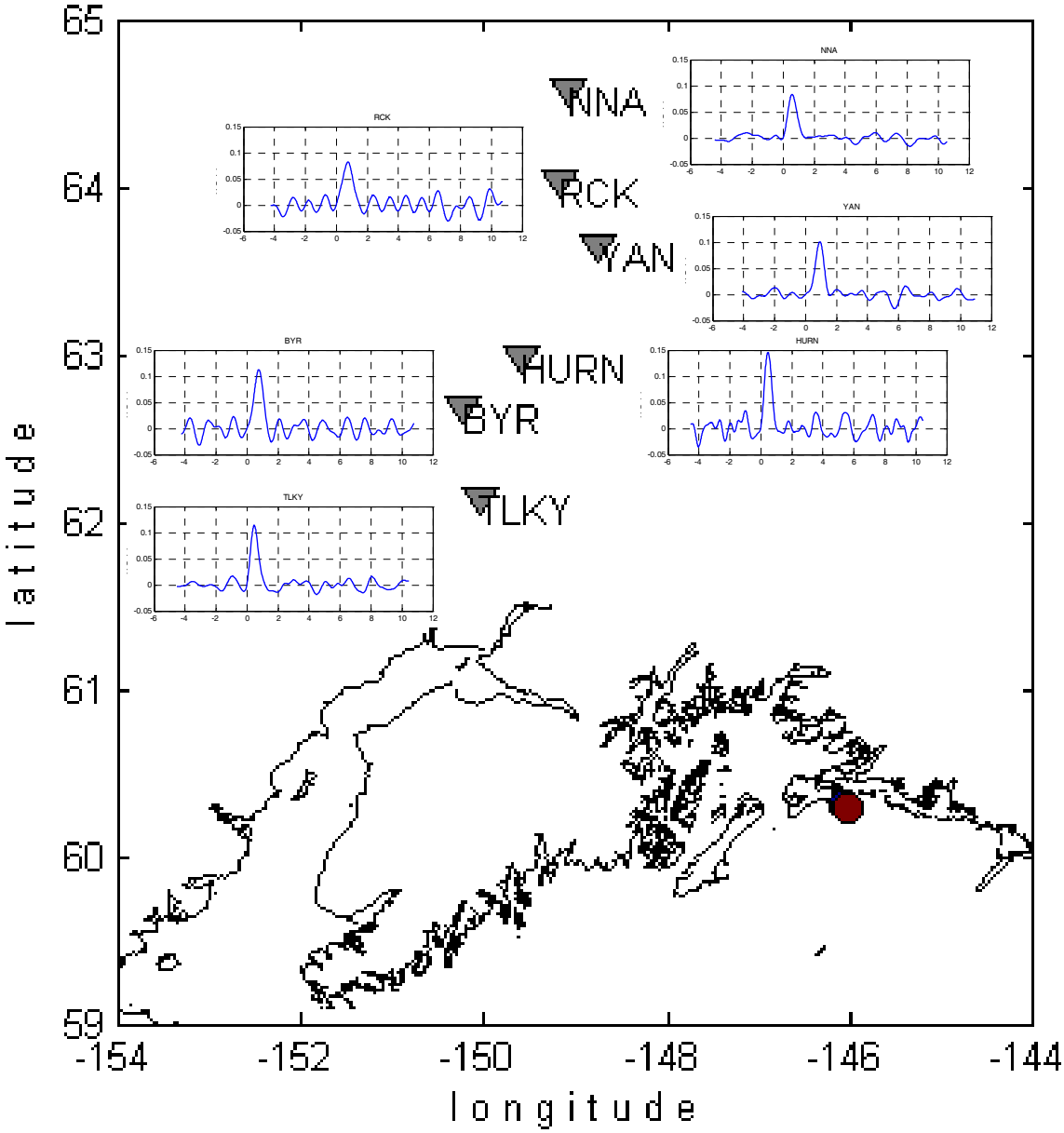

Figure 11. RSTFs for the event pair 9 (mainshock)-8 (EGF) (Table 2). Although the RSTFs are very stable, the station azimuthal coverage is too poor to determine if the event displayed rupture directivity.

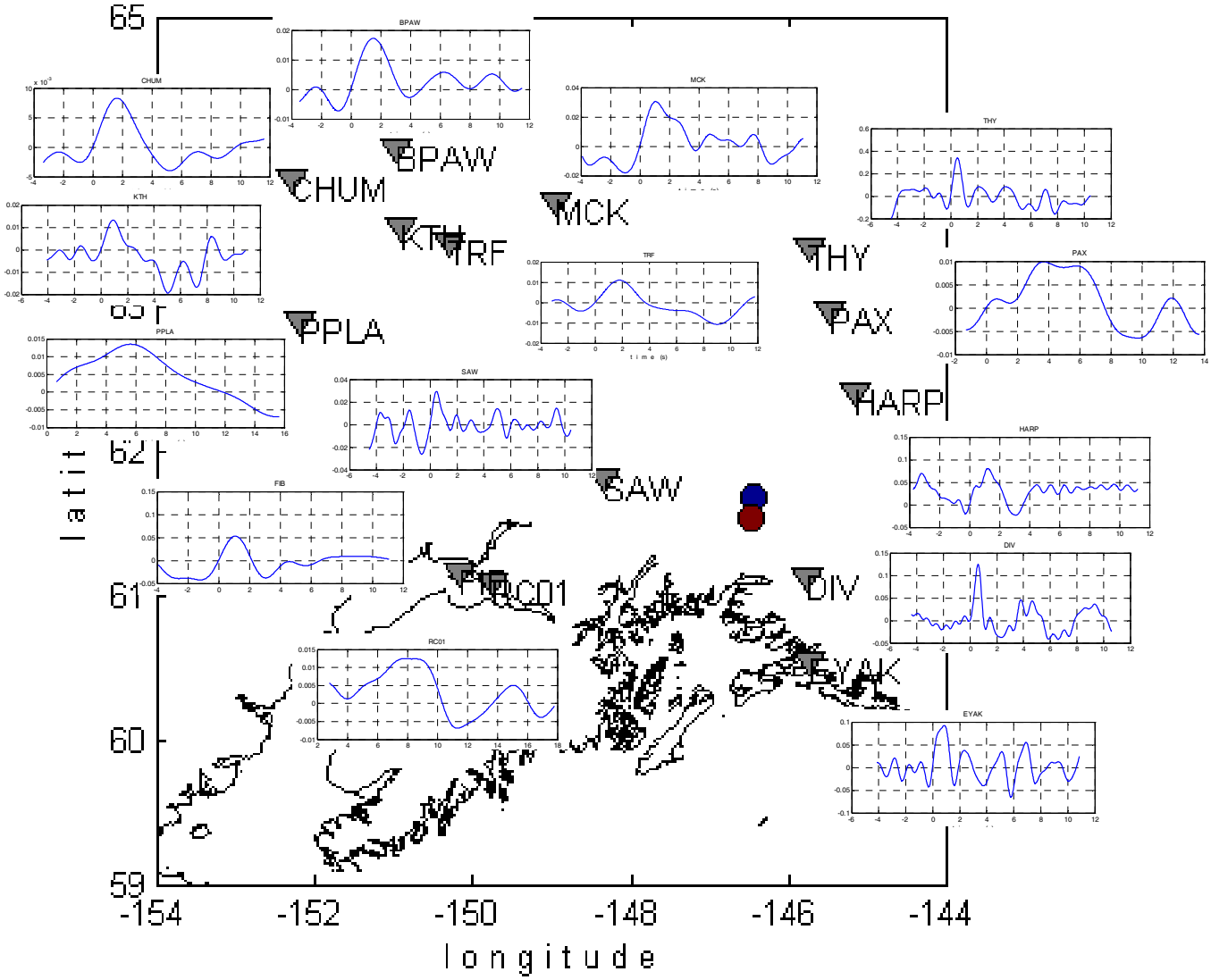

Figure 12. Variability of RSTF depending on the azimuth from the event to the station (event pair 22(mainshock)-26 (EGF), Table 2). The stations PPLA, PAX and RC01 do not show stable RSTFs.

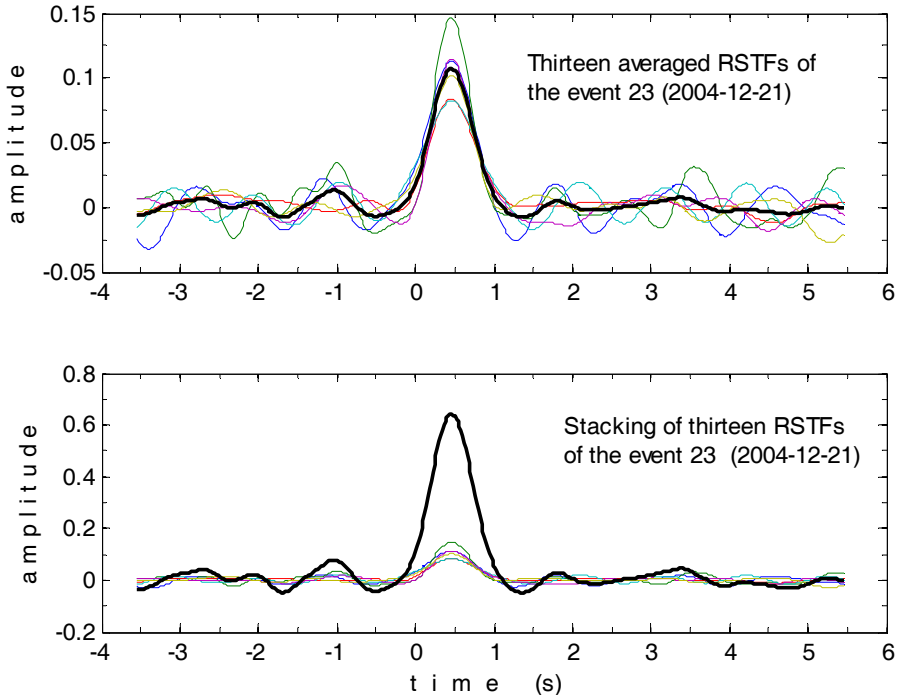

Figure 13. Averaged and stacked RSTFs for event 23 (12-21-2004).

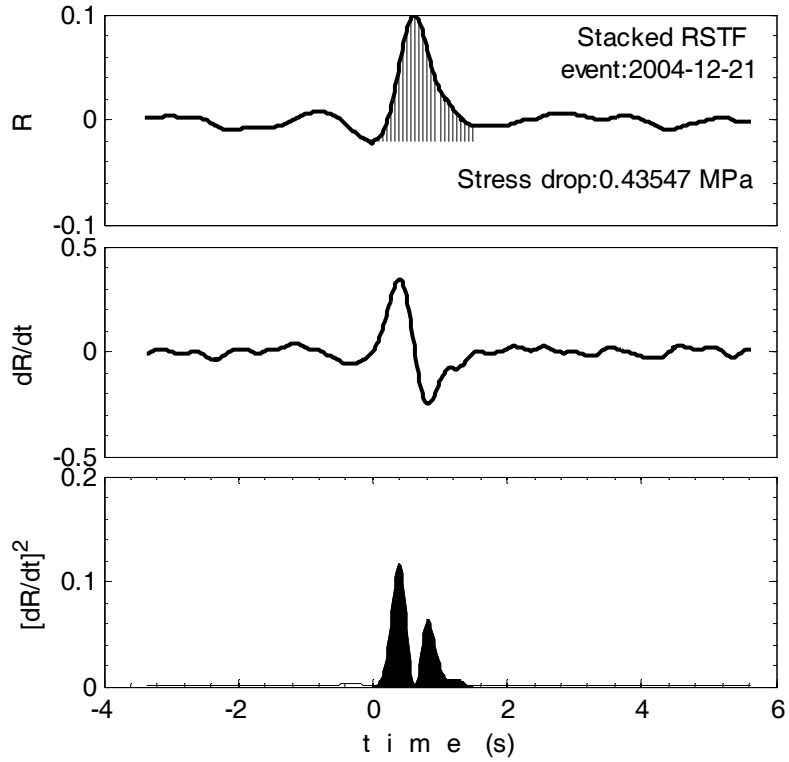

Figure 14. Area under the stacked RSTF for event 23 (top), the derivative of the RSTF (middle) and the derivative squared (bottom) that can be used to calculate the stress drop (see equation 3).

Since all three earthquakes examined are intraslab events, it is appropriate to solve for their stress drops using parameters for oceanic crust/mantle. We assumed a P-wave velocity of 8 km/sec, S-wave velocity of 4.6 km/sec, density of 3.3 g/cm^3 and shear modulus of 6.7 x 10^{10} Pa. Table 3 lists the results for the stress drop analysis. Note that the stress drops for all 3 events are within the range of 0.2 to 0.95 MPa (2 to 9.5 bars). All these events are located beneath the Prince William Sound asperity where coupling across the plate interface should be strong.

Table 3 – Stress drop results

EVENT PAIR	**SEISMIC MOMENT (dyne*cm)**	**Δσ (MPa)**
2000-03-01 / 2000-02-27 (events 9/8)	$1.66 * 10^{24} / 4.51*10^{16}$	0.94
2004-08-25 / 2005-04-06 (events 22/26)	$6.01*10^{23} / 1.81814*10^{16}$	0.21
2004-12-21 / 2005-01-13 (events 23/24)	$4.98*10^{23} / 1.01357*10^{16}$	0.17

Veilleux (2006) determined stress drops using EGF techniques for three events recorded at regional broadband stations in Alaska and Canada. Unlike this study she was only able to obtain estimates from 1 to 2 stations per event. Her results (orange squares) are compared to our preliminary results (blue stars) from Table 3 in Figure 15. In this case we compare the stress drops to the apparent stress relationships found for oceanic regions by Choy and Kirby (2004). Although apparent stress and stress drop are estimated differently they should be proportional to one another. Note that the event with the highest stress drop (V3) occurs within Choy and Kirby's tectonic region IV (cold intraslab events near changes in slab geometry) and is located within the more steeply dipping portion of the slab (Figure 3). Most other events fall within region III (warm intraslab or flat slab), and are near the edge of the Yakutat block or within the flatly dipping portion of the slab (Figure 3).

Crustal events:

The only crustal events that have been recorded well enough to study using the EGF technique occurred prior to the establishment of digital seismographs, with most occurring during the 1930's. Thus we needed to modify existing software to scan and digitize the paper seismograms of these events. We have completed the digitization but need to process EGF in a slightly different manner as the instruments operating at the time did not have modern broadband responses. We plan to present our results at the fall 2008 meeting of the American Geophysical Union.

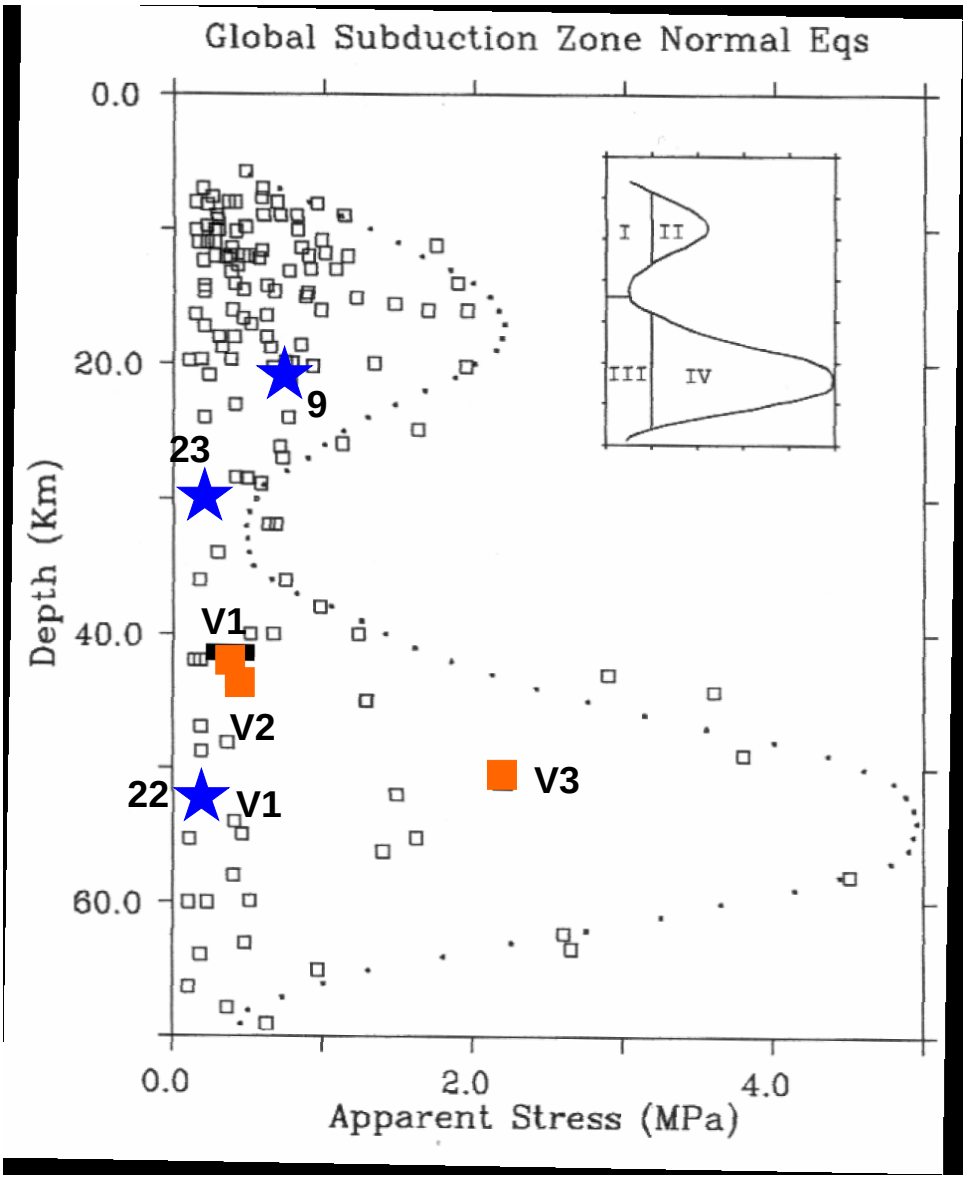

Figure 15 – Stress drops of events of this study (stars, see Table 2 for event locations) and from Veilleux (2006) (squares, see Figure 3 for locations) versus depth. Regions are from Choy and Kirby (2004), see text for details.

Related Studies

A paper that examines the seismicity of Prince William Sound and its relationship to known crustal structure and potential field data will be published in an upcoming AGU Monograph (Doser et al., 2008). A paper relating the seismicity of all of south-central Alaska (144 to 154 W, 58 to 62 N) to crustal structure, seismic tomography and potential field data has been submitted to the Seismological Society of America (Doser and Veilleux, 2008). A manuscript on using intensity information to locate earthquakes in three regions of Alaska is in preparation with preliminary results presented at the spring 2008 meeting of the Seismological Society of America (Doser, 2008). Work continues on studies of southeastern Alaska earthquakes with results presented at the spring 2008 meeting of the Seismological Society of

America (Rodriguez and Doser, 2008; Escudero and Doser, 2008) and earthquakes of interior Alaska. Dr. Doser visited Alaska in May 2008 to discuss research results with colleagues at the U.S. Geological Survey in Anchorage and the University of Alaska-Fairbanks.

Reports Published:

Romero, O.M., and D. I. Doser (2008). Determination of relative source time functions using empirical Greens functions for earthquakes in South-Central Alaska, (abstract), *Seismol. Res. Lett*. **79**, 350.

Romero, O.M., and D.I. Doser (2008). Using relative source time functions to calculate stress drops for earthquakes in south-central Alaska (abstract), to be presented at Fall 2008 meeting of American Geophysical Union.

Availability of Data Sets:

Copies of digital waveform data and digitized historic seismograms are from Dr. Diane Doser, (915)-747-5851 or doser@geo.utep.edu.

Bibliography

Brocher, T.M., G.S. Fuis, M.A. Fisher, G. Plafker, M.J. Moses, J.J. Taber, and N.I. Christensen (1994). Mapping the megathrust beneath the northern Gulf of Alaska using wide-angle seismic data, *J. Geophys. Res.* **99**, 11,663-11,686.

Choy, G.L., and S.H. Kirby (2004). Apparent stress, fault maturity and seismic hazard for normal-fault earthquakes at subduction zone, *Geophys. J. Internat.* **159**, 991-1012.

DeMets, C., and T.H. Dixon (1999). New kinematic models for Pacific-North America motions from 3 Ma to present, 1: Evidence for steady motion and biases in the NUVEL-1A model, *Geophys. Res. Lett.* **26**, 1921-1924.

Doser, D.I., A. de la Peña, and A.M. Veilleux (2008). Seismicity of the Prince William Sound region and its relation to plate structure and the 1964 great Alaska earthquake in "*Active Tectonics and Seismic Potential of Alaska*", J.T. Freymueller, P.J. Haeussler, R.L. Wesson and G. Ekström, editors, **179**, Geophysical Monograph Series, American Geophysical Union.

Doser, D.I., and A.M. Veilleux (2008). A comprehensive study of the seismicity of the Kenai Peninsula-Cook Inlet region, South Central Alaska, submitted to Bull. Seismol. Soc. Amer.

Doser, D.I. (2008). Estimating magnitude and location from intensity for three regions of Alaska, *Seismol. Res. Lett.* **79,** 322.

Eberhart-Phillips, D., D.H. Christensen, T.M. Brocher, R. Hansen, N.A. Ruppert, P.J. Haeussler and G.A. Abers (2006). Imaging the transition from Aleutian subduction to Yakutat collision in central Alaska, with local earthquakes and active source data, *J. Geophys. Res,* **111***,* B11303, doi:10.1029/2005JB004240.

Escudero, C.S., and D.I. Doser (2008). Relative source time function studies of earthquakes in southeastern Alaska, *Seismol. Res. Lett.* **79**, 350.

Houston, H. (1990). Broadband Source Spectrum, Seismic Energy, and Stress Drop of the 1989 Macquarie Ridge Earthquake. *Geophysical Research Letters* **17**, 1021-1024.

Johnson, J.M., K. Satake, S.R. Holdahl, and J. Sauber (1996). The 1964 Prince William Sound earthquake: Joint inversion of tsunami and geodetic data, *J. Geophys. Res.* **101**, 523-532.

Muller, C.S., (1985). Source Pulse Enhancement by Deconvolution of an Empirical Green Function, *Geophysical Research Letters*, **12**, 33-36.

Nava, F. A. (2002). Procesamiento de Series de Tiempo. Fondo de Cultura Económica. Mexico. p. 90-91. ISBN 968-16-6766-2.

Plafker, G., (1987). Regional geology and petroleum potential of the northern Gulf of Alaska continental margin, in D.W. Scholl, A. Grantz, and J.G. Vedder, eds., Geology and Resource Potential of the Continental Margin of Western North America and Adjacent Ocean Basins-Beaufort Sea to Baja California, *Earth Science Series* **6**, 229-268, Circum-Pacific Council for Energy and Mineral Res., Houston, TX.

Rodriguez, H., and D. I. Doser (2008). Earthquake relocation studies in southeastern Alaska, *Seismol. Res. Lett*. **79**, 294

Stover, C.W., and J. L. Coffman (1993). Seismicity of the United States, 1568-1989 (Revised), *U.S. Geological Survey Prof. Pap.* **1527**, 418 pp.

Veilleux, A.M., (2006). Seismicity studies of the Wadati-Benioff zone, south-central Alaska, *Ph.D. dissertation*, Univ. Texas at El Paso, 73 pp.

Velasco, A.A., C.J. Ammon, and T. Lay (1994a). Empirical Green function deconvolution of broadband surface waves: rupture directivity of the 1992 Landers, California (M=7.3) earthquake, *Bull. Seism. Soc. Amer.* **84**, 735-750.

Velasco, A. A., C.J. Ammon and T. Lay (1994b), Recent large earthquakes near Cape Mendocino and in the Gorda Plate: Broadband source time functions, fault orientations, and rupture complexities, *Journal of Geophysical Research* **99**, 711-728.

Walter, W., K. Mayeda, R. Gok, and A. Hofstetter (2006). The scaling of seismic energy with moment; simple models compared with observations, *Geophysical Monograph* **170** (R.E. Abercrombie, A. McGarr, H. Kanamori and G. Di Toro, eds.), 25-41.

Wesson, R.L., A.D. Frankel, C.S. Mueller, and S.C. Harmsen (1999). Probabilistic seismic hazard maps of Alaska, *U.S. Geol. Surv. Open File Rept*. **99-36**, 20 pp.